Non-Hermitian Band Topology and Skin Modes in Active Elastic Media

Colin Scheibner,[1,2] William T. M. Irvine,[1,2,3] and Vincenzo Vitelli[1,2,*]
[1]James Franck Institute, The University of Chicago, Chicago, Illinois 60637, USA
[2]Department of Physics, The University of Chicago, Chicago, Illinois 60637, USA
[3]Enrico Fermi Institute, The University of Chicago, Chicago, Illinois, 60637, USA

(Received 14 January 2020; revised 7 July 2020; accepted 10 August 2020; published 9 September 2020)

Solids built out of active components can exhibit nonreciprocal elastic coefficients that give rise to non-Hermitian wave phenomena. Here, we investigate non-Hermitian effects present at the boundary of two-dimensional active elastic media obeying two general assumptions: their microscopic forces conserve linear momentum and arise only from static deformations. Using continuum equations, we demonstrate the existence of the non-Hermitian skin effect in which the boundary hosts an extensive number of localized modes. Furthermore, lattice models reveal non-Hermitian topological transitions mediated by exceptional rings driven by the activity level of individual bonds.

DOI: 10.1103/PhysRevLett.125.118001

The microscopic injection of energy into solid media via active, living, or robotic components fundamentally alters their mechanical waves [1–7]. As with optics [8,9], topoelectric circuits [10–13], and open quantum systems [14,15], the interplay between activity (gain) and dissipation (loss) can often be captured by non-Hermitian operators [16–18]. In all these contexts, a central question is the role of non-Hermiticity at the boundary of the system. Like their Hermitian counterparts, non-Hermitian systems have been shown to exhibit topological invariants that ensure localized boundary modes [19–32]. However, in some cases, the familiar bulk-boundary correspondence breaks down for non-Hermtian systems. Such systems exhibit the non-Hermitian skin effect, in which an extensive number of modes are localized to the system's boundary [33–35].

Here we examine the non-Hermitian wave phenomena that arise from the elastic properties of a class of active solids. In the continuum, non-Hermiticity enters the linear elasticity of a solid through odd elastic moduli, which are active moduli that violate Maxwell-Betti reciprocity [7]. We show that such odd elastic moduli when combined with anisotropy can give rise to the non-Hermitian skin effect. This effect implies a dramatic localization of vibrational modes to the system's boundary. Furthermore, we take a microscopic view of elasticity by considering 2D lattices composed of active bonds. These bonds, while active, retain two crucial features of Hookean springs: they conserve linear momentum and depend only on changes in relative distance. We uncover a non-Hermitian topological transition driven by the level of activity. This transition differs qualitatively from its Hermitian counterpart in that it is mediated by exceptional rings. Such rings arise due to geometric changes in the particle trajectories that enable the system to draw energy from nonpotential forces. We interpret the resulting energy cycles in terms of a generalized PT symmetry.

Non-Hermitian elasticity.—We choose as our starting point elasticity theory, the continuum description of solids that captures their ability to resist shape change at large length scales [36]. Unlike conventional treatments of passive elasticity, we seek to capture at a coarse-grained level the effects induced by *nonconservative* internal forces $F_i(\mathbf{x})$ satisfying three assumptions [7]. First, the forces conserve linear momentum, and therefore can be written as the divergence of a stress $\partial_j \sigma_{ij}(\mathbf{x})$. Second, the forces only depend on the static change in shape, which is captured by gradients of the displacement field $u_{ij} = \partial_i u_j(\mathbf{x})$. Finally, we employ the phenomenological assumption that the stresses can be approximated as linearly proportional to the displacement gradients: $\sigma_{ij} = C_{ijmn} u_{mn}$. The object C_{ijmn} is the elastic tensor, and it encodes the material's response to static deformation.

Following the approach of Ref. [7], it is useful to express the elastic tensor as the sum of two pieces:

$$C_{ijmn} = C^e_{ijmn} + C^o_{ijmn}, \tag{1}$$

where $C^e_{ijmn} = C^e_{mnij}$ is even, or symmetric, under exchange of pairs of the lower indices while $C^o_{ijmn} = -C^o_{mnij}$ is odd, or antisymmetric [7]. To understand the decomposition, consider the elastic work done (per unit volume) by a patch of material brought through a closed cycle of strain: $w = -\oint \sigma_{ij} du_{ij} = C^o_{ijmn} \oint u_{ij} du_{mn}$. If the system is passive, $w = 0$ for any cycle that begins and ends in the same state, and hence $C^o_{ijmn} = 0$. However, for an active solid, this requirement does not hold and, consequently, C^o_{ijmn} may be nonzero. We use the term "odd elastic media" to refer to this class of active systems [7].

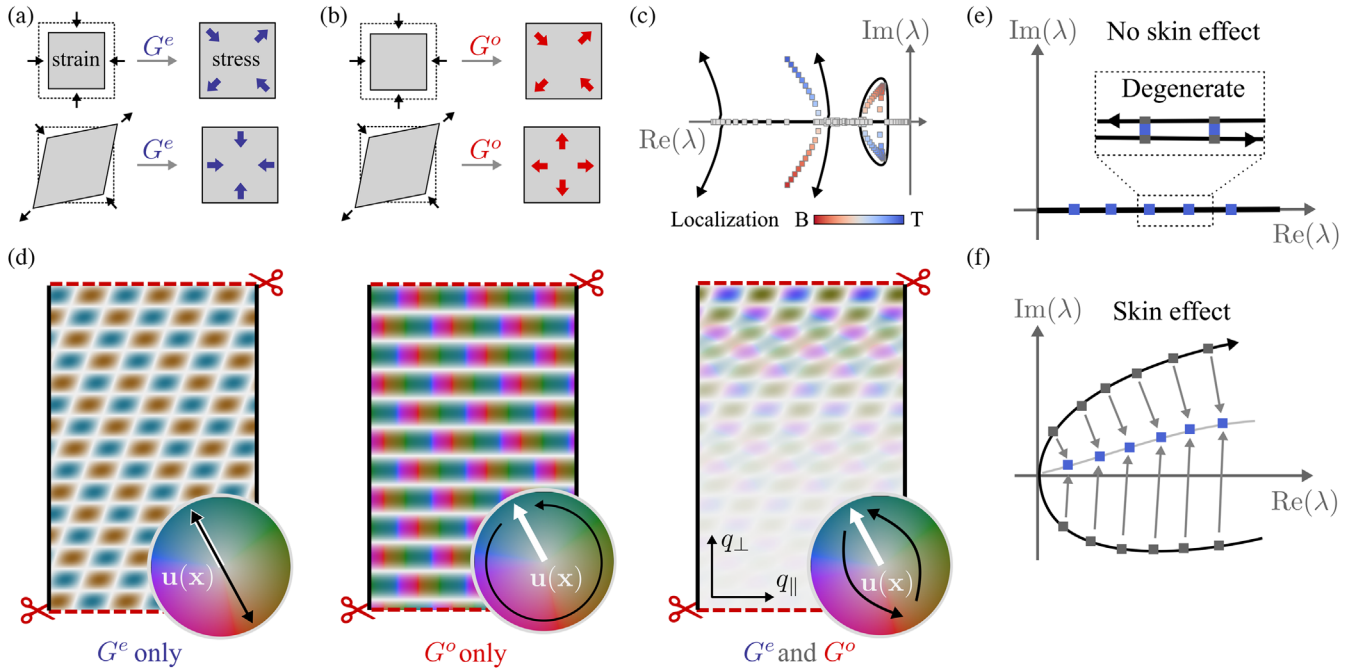

FIG. 1. Elastic non-Hermitian skin effect. (a) An anisotropic, passive elastic modulus G^e that couples dilation and shear. (b) The corresponding anisotropic, odd elastic counterpart G^o. (c) The elastic spectrum for $G^o/G^e = 1.7$. The black arrows are analytical calculations of the periodic boundary spectrum, see [41]. The colored squares denote numerical calculations of the spectrum with open boundary conditions. Blue (red) indicates localization to the top (bottom) boundary. (d) Numerically computed eigenmodes with only G^e present (left), only G^o present (middle), and both G^o and G^o (right). Hue indicates the angle and opacity indicates the magnitude of the displacement field $\mathbf{u}(\mathbf{x})$. The horizontal boundaries (red) are open and the vertical boundaries (black) are periodic. The boundary termination forms an angle $\pi/4$ with respect to the axis of anisotropy. (e) Since the spectrum of a Hermitian system lies on the real line, a generic eigenvalue is at least doubly degenerate. (f) For a non-Hermitian system, the spectrum can trace out nondegenerate arcs (black solid). In this case, the spectrum deforms (blue squares) to form degeneracies when a boundary is introduced.

Suitable experimental platforms include robotic metamaterials [2,5], solids with integrated piezoelectric components [37,38], and chiral optical matter [39–41].

Here, we focus on *anisotropic* odd-elastic media and illustrate how they generically exhibit the non-Hermitian skin effect. For concreteness, consider a minimal example of anisotropic odd elasticity represented by the following pictorial stress-strain relationship (see the Supplemental Material for standard tensor notation [41]):

$$\begin{pmatrix} \text{dilation} \\ \text{shear stress} \\ \text{pressure} \end{pmatrix} = \begin{pmatrix} 0 & 0 & G^e+G^o \\ 0 & \mu & 0 \\ G^e-G^o & 0 & \mu \end{pmatrix} \begin{pmatrix} \text{dilation} \\ \text{shear strain} \\ \text{pressure} \end{pmatrix}. \tag{2}$$

The modulus G^e (contained in C^e_{ijmn}) couples dilation ( ) to shear stress ( ) and shear strain ( ) to pressure ( ) symmetrically, see Fig. 1(a). By contrast, the modulus G^o (contained in C^o_{ijmn}) provides an antisymmetric coupling [Fig. 1(b)]. Equation (2) also includes the standard shear modulus μ to ensure mechanical stability. In the presence of these moduli, the expression for elastic forces may be written as $\mathbf{F}(\mathbf{x}) = \hat{D}\mathbf{u}(\mathbf{x})$, where $\hat{D}$ takes the following form:

$$\hat{D} = \begin{pmatrix} \mu\nabla^2 + 2G^e\partial_x\partial_y & G^e\nabla^2 + G^o[\partial_x^2 - \partial_y^2] \\ G^e\nabla^2 - G^o[\partial_x^2 - \partial_y^2] & \mu\nabla^2 + 2G^e\partial_x\partial_y \end{pmatrix}, \tag{3}$$

where $\nabla^2 = \partial_x^2 + \partial_y^2$. In Eq. (3) we observe that the operator $\hat{D}$ becomes non-Hermitian when G^o is nonzero, i.e., when the anisotropic moduli display an odd component arising from nonconservative elastic forces. We find that the non-Hermiticity has a dramatic effect on the nature of the bulk modes. In Fig. 1(c), we show the spectrum of $\hat{D}$ as a function of wave number q_y for fixed q_x when both G^e and G^o are present. We find two striking features. First, the open boundary spectrum (square markers) differs dramatically from the spectrum with periodic boundaries (black lines). Second, when we examine a typical eigenmode [Fig. 1(d), right] we find that the mode is exponentially localized to the open edge. In Fig. 1(c), we color each mode by the degree of localization to the top (blue) and bottom (red) boundaries. In contrast to typical topological waves or Rayleigh waves in Hermitian systems [36], an extensive number of modes are localized to the boundary. This extensive localization of bulk modes is an elastic manifestation of the non-Hermitian skin effect.

Yet, when either $G^o = 0$ or $G^e = 0$, the skin effect disappears [Fig. 1(d), left and center, respectively]. To gain insight into its origins, we consider the notion of a generalized Brillouin zone [33–35]. Let $q_\parallel$ ($q_\perp$) be the wave number parallel (perpendicular) to the boundary. For a finite system, at least two Bloch modes must have the same eigenvalue λ and wave number $q_\parallel$ in order to interfere to satisfy a given boundary condition, e.g., $\mathbf{u} = 0$. If $\hat{D}$ is Hermitian or anti-Hermitian, this condition is generically satisfied since the spectrum is confined to lie entirely along the real or imaginary line [Fig. 1(e)]. However, when both C^e_{ijmn} and C^o_{ijmn} are nonzero, the spectrum can inhabit the full complex plane. Consequently, the spectrum, plotted as a function of $q_\perp$, need not retrace itself [Fig. 1(f)]. In this case, there exist segments in which no two extended Bloch modes have the same λ and $q_\parallel$. Nonetheless, one can consider Bloch modes with complex wave numbers $\tilde{q}_\perp = q_\perp + i\kappa(q_\perp)$. By analytically continuing $\hat{D}$ into the complex Brillouin zone, the eigenvalues flow together to enable interference at the boundary.

Finally, we note that the use of the two specific moduli G^e and G^o in Eq. (2) is purely illustrative. More generally, two necessary conditions must be met in order for the non-Hermitian skin effect to emerge within the continuum description of an elastic medium. First, both C^e_{ijmn} and C^o_{ijmn} must be nonzero for the spectrum to occupy the complex plane. Second, the system must be anisotropic in order for the spectrum not have a reflection symmetry over the system's boundary ($q_\perp \mapsto -q_\perp$), see the Supplemental Material [41]. For the example in Eq. (2), both C^e_{ijmn} and C^o_{ijmn} are independently anisotropic. In the Supplemental Material we examine a case in which only C^e_{ijmn} is anisotropic. Finally, we note that $\hat{D}$ has inversion symmetry, which implies that the skin modes occur in pairs localized to each boundary [12]. This is a contrast to systems in which an external medium enables an effective violation of Newton's third law [4–6]. The continuum limit of these systems (whose interactions do not conserve linear momentum) yields $\hat{D} \propto q$, rather than the $\hat{D} \propto q^2$ dependence characteristic of elasticity [41].

Microscopic model.—A ubiquitous minimal model for elastic solids is a collection of masses connected by Hookean springs [53–66]. The Hookean spring captures two generic features of elasticity. First, the interaction conserves linear momentum, since the forces on the two participating particles are equal and opposite. Second, the force only depends on the change in bond length. Hence, the emerging mechanical response will be sensitive only to intrinsic changes in geometry. Yet, the Hookean spring has an additional feature built in: its force law follows from the gradient of a potential. Here, we retain the assumptions of length dependence and linear momentum conservation, and we study the most general 2D linear pairwise interaction when only energy conservation is lifted [7]:

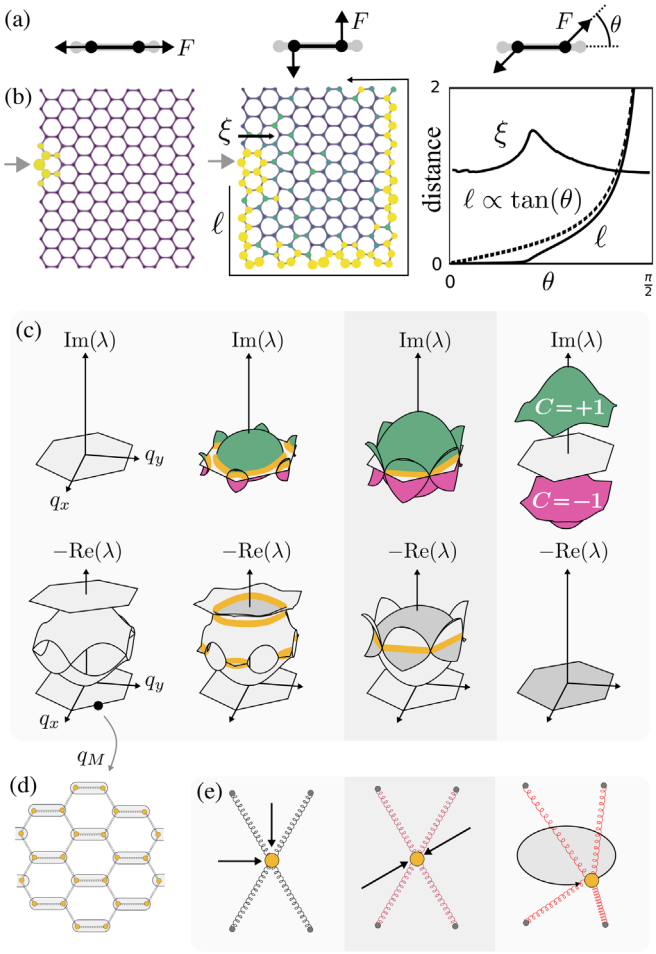

FIG. 2. Non-Hermitian topological transition and exceptional rings. (a) The generalized Hookean spring with the force $\mathbf{F}$ oriented at an angle θ with respect to the bond vector. (b) Simulations with $\theta = 0$ (left) and $\theta = \pi/2$ (right) in which a particle at the edge is vibrated. Two lengths, the penetration depth ξ and the propagation distance ℓ, are plotted as a function of θ. (c) The spectrum plotted over the Brillouin zone for $\theta = 0, \pi/12, \pi/6, \pi/2$. Regions of positive (green) and negative (purple) Berry curvature are highlighted. The orange lines denote exceptional rings. (d) At point $\mathbf{q}_M$, pairs of masses move in tandem. (e) The eigenmodes (arrows) of the effective single particle system at $\theta = 0, \pi/6, \pi/2$.

$$\mathbf{F}(r) = -(k\hat{\mathbf{r}} + k^a\hat{\boldsymbol{\phi}})\delta r, \tag{4}$$

where $\hat{\mathbf{r}}$ ($\hat{\boldsymbol{\phi}}$) is a unit vector pointing along (transverse to) the bond vector, δr is the change in length of the bond, and k and k^a are spring constants [see Fig. 2(a)].

When the bond is taken on a closed cycle, the work done $W = \oint \mathbf{F} \cdot d\mathbf{r}$ is equal to k^a times the area enclosed by the path. Hence, when $k^a \neq 0$, Eq. (4) cannot be derived from a potential. In principle, Eq. (4) can be paired with any form of dynamics that governs the temporal evolution of the system. Here, for concreteness, we will interpret our results in the context of an overdamped equation of motion:

$\Gamma\partial_t\mathbf{u} = \mathbf{F}$, where $\mathbf{u}$ is the displacement of the particle and Γ is a drag coefficient. By adjusting the angle $\theta = \arctan(k^a/k)$ between $\hat{\mathbf{r}}$ and $\mathbf{F}$, we can interpolate between longitudinal and transverse interactions [67–76]. In the Supplemental Material [41], we show how the equations governing the *overdamped* dynamics of an active solid with *nonconservative* bonds described by Eq. (4) are the same as those governing the *inertial* dynamics of a gyroscopic metamaterial [77–81] with *conservative* springlike interactions and weak dissipation. However, we note that deformation cycles performed with the gyroscopic media do not extract energy since the left-hand side of Eq. (4) represents torques, not forces. Similarly, in the continuum treatment of gyroscopes, the left-hand side of Eq. (2) represents angular momentum currents, not stresses.

Generalized PT symmetry and energy cycles.—For a generic network of masses connected by the bonds in Eq. (4), the linear relationship between forces $\mathbf{F}(\mathbf{x})$ and displacements $\mathbf{u}(\mathbf{x})$ can be captured by a dynamical matrix formalism $\mathbf{F}(\mathbf{x}) = \sum_{\mathbf{x}'} D(\mathbf{x},\mathbf{x}')\mathbf{u}(\mathbf{x}')$, where $\mathbf{x}$ and $\mathbf{x}'$ are lattice sites and $D(\mathbf{x},\mathbf{x}')$ is the dynamical matrix. The mere fact that the forces and displacements are real implies that $[\mathcal{K}, D(\mathbf{x},\mathbf{x}')] = 0$, where $\mathcal{K}$ is complex conjugation. Since $\mathcal{K}$ is an antiunitary operator with $\mathcal{K}^2 = 1$, we say that the dynamical matrix has a generalized PT symmetry [17,82–84], see [41].

The PT symmetry has the following physical consequence: if a given eigenvalue λ of D is real, then the corresponding eigenvector $\mathbf{u}_\lambda(\mathbf{x})$ may be chosen real. Since $\mathbf{u}_\lambda(\mathbf{x})$ is real, the corresponding trajectory of each particle traces out straight lines in time [Fig. 2(e), left]. Moreover, nonreal eigenvalues come in complex conjugate pairs $\lambda_\pm = \lambda_R \pm i\lambda_I$ with eigenvectors of the form:

$$\mathbf{u}_{\lambda_\pm}(\mathbf{x}) = \mathbf{v}(\mathbf{x}) \pm i\mathbf{w}(\mathbf{x}), \tag{5}$$

where $\mathbf{v}(\mathbf{x})$ and $\mathbf{w}(\mathbf{x})$ are real vectors. Physically, a complex eigenvalue indicates energetic gain or loss. In this case, the eigenmode cycles between two states $\mathbf{v}(\mathbf{x})$ and $\mathbf{w}(\mathbf{x})$. Since the bonds are nonpotential, the cycles result in the injection (or removal) of energy [Fig. 2(e), right]. If all the eigenvalues of D are real, we say that D is PT unbroken, and PT broken otherwise [85].

Non-Hermitian topological transition.—Given a microscopic model, we can study not only the acoustic bands (accessible within the continuum theory) but also features of the optical bands. Figure 2(b) shows the response of a honeycomb lattice to vibrations applied at the boundary in two extreme cases: the passive Hookean limit $\theta = 0$, and the active transverse limit $\theta = \pi/2$. In the transverse limit, we see the emergence of a sustained, unidirectional edge wave characteristic of a Chern insulator [77,78]. Due to the translation symmetry, we may express the dynamical matrix in terms of wave number $\mathbf{q}$ [41]:

$$D_\theta(\mathbf{q}) = \cos(\theta)D_0(\mathbf{q}) + \sin(\theta)D_{\pi/2}(\mathbf{q}). \tag{6}$$

For Hermitian systems, nontrivial topology requires breaking time-reversal symmetry (TRS): $D_\theta(-\mathbf{q}) = D_\theta^*(\mathbf{q})$ [86]. However, here $D_\theta(\mathbf{q})$ naïvely obeys TRS for all θ since the forces and displacements are real quantities. Nonetheless, band topology is still possible due to the violation of Hermiticity. At $\theta = \pi/2$, the dynamical matrix $D_{\pi/2}(\mathbf{q})$ (restricted to its optical bands, see [41]) is anti-Hermitian. Hence the relevant Hermitian Hamiltonian $H(\mathbf{q}) = iD_{\pi/2}(\mathbf{q})$ violates TRS as required. When $\theta = \pi/2$, the lattice boundary hosts a chiral edge state due to the nonvanishing Chern numbers of the optical bands.

The transition between Hermitian and anti-Hermitian limits is accompanied by two length scales ξ and ℓ [Fig. 2(b), right]. The first length scale ξ is the penetration depth into the medium, which is set by the structure of the *eigenvectors* of D_θ. Like the Haldane model [41,87,88], ξ is roughly constant as the gap opens and closes. Yet, the edge modes do not become visible until large values of θ are probed. This effect can be traced to the second length scale ℓ, which is the distance the wave propagates around the edge. This length scale is set by the *eigenvalues* of the dynamical matrix. For a given mode, $\ell \approx \tau\omega/q$, where $\tau = -1/\mathrm{Re}(\lambda)$ is the decay rate and $\omega = -\mathrm{Im}(\lambda)$ is the oscillation frequency. Hence, the localized edge mode becomes apparent close to the anti-Hermitian limit, i.e., θ near $\pi/2$.

Mechanical exceptional points.—Insight into the transition is gained by examining the point $\mathbf{q}_M$ in the Brillouin zone. At this point, the 4×4 dynamical matrix $D(\mathbf{q}_M)$ can be reduced to an effective dynamical matrix that governs the motion of a single particle in a trap [Figs. 2(d) and 2(e)]:

$$D_{\mathrm{eff}} = -\begin{pmatrix} \cos\theta & -3\sin\theta \\ \sin\theta & 3\cos\theta \end{pmatrix}, \tag{7}$$

with eigenvalues $\lambda_\pm = -2\cos\theta \pm \sqrt{2\cos(2\theta) - 1}$, see [41]. For $\theta < \pi/6$, two real modes exist that trace out straight lines [Fig. 2(e), left]; for $\theta > \pi/6$, the eigenmodes trace out cycles (right). At the transition $\theta = \pi/6$, D_{eff} permits only a single eigenvalue $\lambda_- = \lambda_+$. However, the anisotropy of the trap and the chirality of the bonds imply that no two linear eigenmodes can have the same eigenvalue unless they are parallel. Hence, the two independent modes coalesce, indicating that the dynamical matrix is defective (i.e., nondiagonalizable). Such occurrences, known as "exceptional points," are generic features of transitions between PT-broken and PT-unbroken phases [15,30,82,89–92]. Here, the exceptional points take on a clear physical meaning: they mark the crossovers between eigenmodes with linear motion, and eigenmodes with circular motion necessary to sustain active waves.

For the honeycomb lattice, the exceptional points do not merely occur at point $\mathbf{q}_M$. Rather, they occur along 1D rings

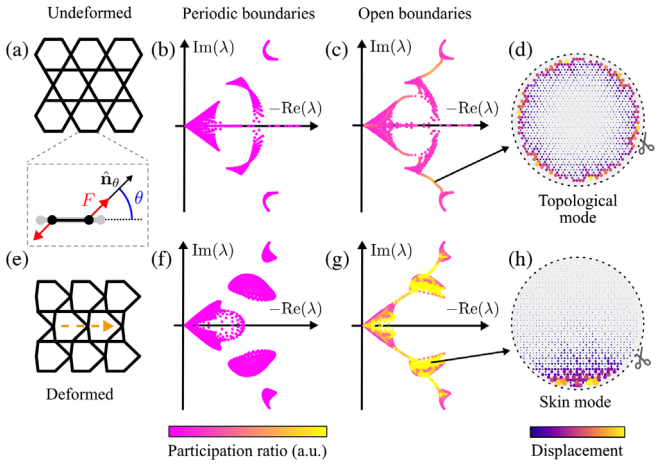

FIG. 3. Microscopic model and skin effect. (a) An undeformed kagome lattice with generalized Hookean springs. Inset: the force law displayed in Eq. (4). (b) The spectrum of a lattice with periodic boundaries. (c) The spectrum of a circle with pinned boundaries. (d) A topological edge mode with displacements visualized by size and color. (e) A deformed kagome lattice. Due to the chirality in the spring, deformation breaks reflection over horizontal axis. (f) The periodic spectrum. (g) The spectrum with open boundaries. (h) Visualization of the non-Hermitian skin mode. In the examples shown, $\theta = 70°$.

depicted in orange in Fig. 2(c). In the Supplemental Material [41], we show that the inversion symmetry of the honeycomb lattice gives rise to a second manifestation of PT symmetry, given by $PT = \mathcal{K}U$, where $U = 1 \otimes \sigma_x$ acts on $D_\theta(\mathbf{q})$. This PT symmetry applies locally at each point in the Brillouin zone. Hence contiguous regions of the Brillouin zone form PT-broken and PT-unbroken phases bounded by rings of exceptional points [3,31,93,94].

Non-Hermitian edge modes.—Finally, we note that the skin effect, previously discussed in the long-wavelength limit within continuum theory, has a counterpart in the optical bands of the lattice models. In Fig. 3, we place the active bonds on an undeformed kagome lattice illustrated in Fig. 3(a) and compute the spectrum with periodic [Fig. 3(b)] and open [Fig. 3(c)] boundaries. We color the modes by their participation ratio $\sum_{\mathbf{x}} |\mathbf{u}(\mathbf{x})|^4$, which serves as a proxy for localization [95]. For the undeformed kagome lattice, the sole difference between the periodic and open boundary spectra is the presence of a subextensive number of localized topological modes that span the band gaps. However, when we introduce a small deformation to the kagome lattice [Figs. 3(e)–3(g)], we observe a dramatic departure [96]. We find that the open boundary system not only contains gap-spanning boundary modes, but the bulk bands become highly localized and their distribution in the complex plane changes dramatically. It is instructive to note the qualitative difference between the topological and skin modes [Figs. 3(d) and 3(h)]. The localized bulk modes are confined to a single direction, whereas the topological modes are confined to all boundaries and decay into the bulk.

Conclusions.—Our work brings to light the non-Hermitian phenomena that arise at the boundary of elastic media for which energetic sources (powered by internal activity or external fields) modify the relationship between static deformation and stress.

V. V. was supported by the Complex Dynamics and Systems Program of the Army Research Office under Grant No. W911NF-19-1-0268. W. T. M. I. and V. V. acknowledge support through the Chicago Materials Research Science and Engineering Center, funded by the NSF through Grant No. DMR-1420709. C. S. was supported by the National Science Foundation Graduate Research Fellowship under Grant No. 1746045. W. T. M. I. acknowledges support from NSF EFRI NewLAW Grant No. 1741685 and NSF DMR Grant No. 1905974. We would like to thank A. Souslov, M. Fruchart, S. Huber, R. Thomale, and the anonymous referee for helpful discussions and useful suggestions.

*vitelli@uchicago.edu

[1] G. Shmuel and N. Moiseyev, Linking scalar elastodynamics and non-hermitian quantum mechanics, Phys. Rev. Applied **13**, 024074 (2020).
[2] M. Brandenbourger, X. Locsin, E. Lerner, and C. Coulais, Non-reciprocal robotic metamaterials, Nat. Commun. **10**, 4608 (2019).
[3] T. Yoshida and Y. Hatsugai, Exceptional rings protected by emergent symmetry for mechanical systems, Phys. Rev. B **100**, 054109 (2019).
[4] M. I. N. Rosa and M. Ruzzene, Dynamics and topology of non-hermitian elastic lattices with non-local feedback control interactions, New J. Phys. **22**, 053004 (2020).
[5] A. Ghatak, M. Brandenbourger, J. van Wezel, and C. Coulais, Observation of non-hermitian topology and its bulk-edge correspondence, arXiv:1907.11619v1.
[6] D. Zhou and J. Zhang, Non-hermitian topological metamaterials with odd elasticity, Phys. Rev. Research **2**, 023173 (2020).
[7] C. Scheibner, A. Souslov, D. Banerjee, P. Surówka, W. T. M. Irvine, and V. Vitelli, Odd elasticity, Nat. Phys. **16**, 475 (2020).
[8] M. Li, X. Ni, M. Weiner, A. Alù, and A. B. Khanikaev, Topological phases and nonreciprocal edge states in non-hermitian floquet insulators, Phys. Rev. B **100**, 045423 (2019).
[9] D. L. Sounas and A. Alu, Non-reciprocal photonics based on time modulation, Nat. Photonics **11**, 774 (2017).
[10] T. Kotwal *et al.*, Active topolectrical circuits, arXiv: 1903.10130.
[11] T. Helbig, T. Hofmann, S. Imhof, M. Abdelghany, T. Kiessling, L. W. Molenkamp, C. H. Lee, A. Szameit, M. Greiter, and R. Thomale, Generalized bulk-boundary correspondence in non-Hermitian topolectrical circuits, Nat. Phys. **16**, 747 (2020).

[12] T. Hofmann *et al.*, Reciprocal skin effect and its realization in a topolectrical circuit, Phys. Rev. Research **2**, 023265 (2020).
[13] T. Yoshida, T. Mizoguchi, and Y. Hatsugai, Mirror skin effect and its electric circuit simulation, Phys. Rev. Research **2**, 022062 (2020).
[14] Y.-X. Wang and A. A. Clerk, Non-hermitian dynamics without dissipation in quantum systems, Phys. Rev. A **99**, 063834 (2019).
[15] H.-K. Lau and A. A. Clerk, Fundamental limits and non-reciprocal approaches in non-hermitian quantum sensing, Nat. Commun. **9**, 4320 (2018).
[16] E. J. Bergholtz, J. C. Budich, and F. K. Kunst, Exceptional topology of non-hermitian systems, arXiv:1912.10048.
[17] Y. Ashida, Z. Gong, and M. Ueda, Non-hermitian physics, arXiv:2006.01837.
[18] N. Hatano and D. R. Nelson, Localization Transitions in Non-Hermitian Quantum Mechanics, Phys. Rev. Lett. **77**, 570 (1996).
[19] S. Yao, F. Song, and Z. Wang, Non-Hermitian Chern Bands, Phys. Rev. Lett. **121**, 136802 (2018).
[20] S. Yao and Z. Wang, Edge States and Topological Invariants of Non-Hermitian Systems, Phys. Rev. Lett. **121**, 086803 (2018).
[21] F. K. Kunst and V. Dwivedi, Non-hermitian systems and topology: A transfer-matrix perspective, Phys. Rev. B **99**, 245116 (2019).
[22] F. K. Kunst, E. Edvardsson, J. C. Budich, and E. J. Bergholtz, Biorthogonal Bulk-Boundary Correspondence in Non-Hermitian Systems, Phys. Rev. Lett. **121**, 026808 (2018).
[23] L. E. F. F. Torres, Perspective on topological states of non-hermitian lattices, J. Phys. Mater. **3**, 014002 (2019).
[24] H. Shen, B. Zhen, and L. Fu, Topological Band Theory for Non-Hermitian Hamiltonians, Phys. Rev. Lett. **120**, 146402 (2018).
[25] L. Li, C. H. Lee, and J. Gong, Geometric characterization of non-hermitian topological systems through the singularity ring in pseudospin vector space, Phys. Rev. B **100**, 075403 (2019).
[26] L. Herviou, J. H. Bardarson, and N. Regnault, Defining a bulk-edge correspondence for non-hermitian Hamiltonians via singular-value decomposition, Phys. Rev. A **99**, 052118 (2019).
[27] K. Kawabata, K. Shiozaki, M. Ueda, and M. Sato, Symmetry and Topology in Non-Hermitian Physics, Phys. Rev. X **9**, 041015 (2019).
[28] K. Kawabata, S. Higashikawa, Z. Gong, Y. Ashida, and M. Ueda, Topological unification of time-reversal and particle-hole symmetries in non-hermitian physics, Nat. Commun. **10**, 297 (2019).
[29] Z. Gong, Y. Ashida, K. Kawabata, K. Takasan, S. Higashikawa, and M. Ueda, Topological Phases of Non-Hermitian Systems, Phys. Rev. X **8**, 031079 (2018).
[30] A. Ghatak and T. Das, New topological invariants in non-hermitian systems, J. Phys. Condens. Matter **31**, 263001 (2019).
[31] J. C. Budich, J. Carlström, F. K. Kunst, and E. J. Bergholtz, Symmetry-protected nodal phases in non-hermitian systems, Phys. Rev. B **99**, 041406(R) (2019).
[32] K. L. Zhang, H. C. Wu, L. Jin, and Z. Song, Topological phase transition independent of system non-hermiticity, Phys. Rev. B **100**, 045141 (2019).
[33] C. H. Lee and R. Thomale, Anatomy of skin modes and topology in non-hermitian systems, Phys. Rev. B **99**, 201103(R) (2019).
[34] C. H. Lee, L. li, R. Thomale, and J. Gong, Unraveling non-hermitian pumping: Emergent spectral singularities and anomalous responses, arXiv:1912.06974 [Phys. Rev. B (to be published)].
[35] D. S. Borgnia, A. J. Kruchkov, and R. J. Slager, Non-Hermitian Boundary Modes and Topology, Phys. Rev. Lett. **124**, 056802 (2020).
[36] L. Landau *et al.*, *Theory of Elasticity*, Course of Theoretical Physics (Elsevier Science, Oxford, 1986).
[37] Y. Y. Chen, R. Zhu, M. V. Barnhart, and G. L. Huang, Enhanced flexural wave sensing by adaptive gradient-index metamaterials, Sci. Rep. **6**, 35048 (2016).
[38] Y. Y. Chen, G. K. Hu, and G. L. Huang, An adaptive metamaterial beam with hybrid shunting circuits for extremely broadband control of flexural waves, Smart Mater. Struct. **25**, 105036 (2016).
[39] Z. Yan, S. K. Gray, and N. F. Scherer, Potential energy surfaces and reaction pathways for light-mediated self-organization of metal nanoparticle clusters, Nat. Commun. **5**, 3751 (2014).
[40] F. Han, J. A. Parker, Y. Yifat, C. Peterson, S. K. Gray, N. F. Scherer, and Z. Yan, Crossover from positive to negative optical torque in mesoscale optical matter, Nat. Commun. **9**, 4897 (2018).
[41] See the Supplemental Material at http://link.aps.org/supplemental/10.1103/PhysRevLett.125.118001 for additional discussion, including a discussion of the nondivergent penetration depth at the gap closing transition in the Haldane model, and including Refs. [42–52].
[42] C. Benzoni, B. Jeevanesan, and S. Moroz, Rayleigh edge waves in two-dimensional chiral crystals, arXiv:2004.09517.
[43] T. Beatus, T. Tlusty, and R. Bar-Ziv, Phonons in a one-dimensional microfluidic crystal, Nat. Phys. **2**, 743 (2006).
[44] D. L. White, Amplification of ultrasonic waves in piezoelectric semiconductors, J. Appl. Phys. **33**, 2547 (1962).
[45] R. Lakes, *Viscoelastic Materials* (Cambridge University Press, Cambridge, England, 2009).
[46] R. Lakes, Elastic and viscoelastic behavior of chiral materials, Int. J. Mech. Sci. **43**, 1579 (2001).
[47] R. S. Lakes, Physical meaning of elastic constants in cosserat, void, and microstretch elasticity, J. Mech. Mater. Struct. **11**, 217 (2016).
[48] A. Souslov, B. C. van Zuiden, D. Bartolo, and V. Vitelli, Topological sound in active-liquid metamaterials, Nat. Phys. **13**, 1091 (2017).
[49] J. Prost, F. Jülicher, and J. Joanny, Active gel physics, Nat. Phys. **11**, 111 (2015).
[50] M. Fruchart and D. Carpentier, An introduction to topological insulators, C. R. Phys. **14**, 779 (2013).
[51] T. Fukui, Y. Hatsugai, and H. Suzuki, Chern numbers in discretized Brillouin zone: Efficient method of computing (spin) Hall conductances, J. Phys. Soc. Jpn. **74**, 1674 (2005).

[52] D. Bernard and A. LeClair, *A Classification of Non-Hermitian Random Matrices* (Springer, Dordrecht, 2002), pp. 207–214.

[53] J. Paulose, B. G.-g. Chen, and V. Vitelli, Topological modes bound to dislocations in mechanical metamaterials, Nat. Phys. **11**, 153 (2015).

[54] J. Paulose, A. S. Meeussen, and V. Vitelli, Selective buckling via states of self-stress in topological metamaterials, Proc. Natl. Acad. Sci. U.S.A. **112**, 7639 (2015).

[55] D. Z. Rocklin, S. Zhou, K. Sun, and X. Mao, Transformable topological mechanical metamaterials, Nat. Commun. **8**, 14201 (2017).

[56] B. G.-g. Chen, N. Upadhyaya, and V. Vitelli, Nonlinear conduction via solitons in a topological mechanical insulator, Proc. Natl. Acad. Sci. U.S.A. **111**, 13004 (2014).

[57] S. Guest and J. Hutchinson, On the determinacy of repetitive structures, J. Mech. Phys. Solids **51**, 383 (2003).

[58] D. Z. Rocklin, B. G.-g. Chen, M. Falk, V. Vitelli, and T. C. Lubensky, Mechanical Weyl Modes in Topological Maxwell Lattices, Phys. Rev. Lett. **116**, 135503 (2016).

[59] A. S. Meeussen, J. Paulose, and V. Vitelli, Geared Topological Metamaterials with Tunable Mechanical Stability, Phys. Rev. X **6**, 041029 (2016).

[60] D. Z. Rocklin, S. Zhou, K. Sun, and X. Mao, Transformable topological mechanical metamaterials, Nat. Commun. **8**, 14201 (2017).

[61] C. L. Kane and T. C. Lubensky, Topological boundary modes in isostatic lattices, Nat. Phys. **10**, 39 (2014).

[62] M. Fruchart, Y. Zhou, and V. Vitelli, Dualities and non-Abelian mechanics, Nature (London) **577**, 636 (2020).

[63] S. D. Huber, Topological mechanics, Nat. Phys. **12**, 621 (2016).

[64] B. G.-g. Chen, B. Liu, A. A. Evans, J. Paulose, I. Cohen, V. Vitelli, and C. D. Santangelo, Topological Mechanics of Origami and Kirigami, Phys. Rev. Lett. **116**, 135501 (2016).

[65] T. C. Lubensky, C. L. Kane, X. Mao, A. Souslov, and K. Sun, Phonons and elasticity in critically coordinated lattices, Rep. Prog. Phys. **78**, 073901 (2015).

[66] K. Sun, A. Souslov, X. Mao, and T. C. Lubensky, Surface phonons, elastic response, and conformal invariance in twisted kagome lattices, Proc. Natl. Acad. Sci. U.S.A. **109**, 12369 (2012).

[67] P. Wiegmann and A. G. Abanov, Anomalous Hydrodynamics of Two-Dimensional Vortex Fluids, Phys. Rev. Lett. **113**, 034501 (2014).

[68] B. C. van Zuiden, J. Paulose, W. T, M. Irvine, D. Bartolo, and V. Vitelli, Spatiotemporal order and emergent edge currents in active spinner materials, Proc. Natl. Acad. Sci. U.S.A. **113**, 12919 (2016).

[69] M. Han, M. Fruchart, C. Scheibner, S. Vaikuntanathan, W. Irvine, J. de Pablo, and V. Vitelli, Statistical mechanics of a chiral active fluid, arXiv:2002.07679.

[70] D. Banerjee, A. Souslov, A. G. Abanov, and V. Vitelli, Odd viscosity in chiral active fluids, Nat. Commun. **8**, 1573 (2017).

[71] A. Galda and V. M. Vinokur, Parity-time symmetry breaking in magnetic systems, Phys. Rev. B **94**, 020408(R) (2016).

[72] A. Souslov, A. Gromov, and V. Vitelli, Anisotropic odd viscosity via a time-modulated drive, Phys. Rev. E **101**, 052606 (2020).

[73] V. Soni, E. Bililign, S. Magkiriadou, S. Sacanna, D. Bartolo, M. J. Shelley, W. T. M. Irvine, The free surface of a colloidal chiral fluid: Waves and instabilities from odd stress and hall viscosity, Nat. Phys. **15**, 1188 (2019).

[74] J. E. Avron, Odd viscosity, J. Stat. Phys. **92**, 543 (1998).

[75] K. Sone and Y. Ashida, Anomalous Topological Active Matter, Phys. Rev. Lett. **123**, 205502 (2019).

[76] K. Sone, Y. Ashida, and T. Sagawa, Exceptional non-hermitian topological edge mode and its application to active matter, arXiv:1912.09055.

[77] L. M. Nash, D. Kleckner, A. Read, V. Vitelli, A. M. Turner, and W. T. M. Irvine, Topological mechanics of gyroscopic metamaterials, Proc. Natl. Acad. Sci. U.S.A. **112**, 14495 (2015).

[78] P. Wang, L. Lu, and K. Bertoldi, Topological Phononic Crystals with One-Way Elastic Edge Waves, Phys. Rev. Lett. **115**, 104302 (2015).

[79] N. P. Mitchell, L. M. Nash, and W. T. M. Irvine, Tunable band topology in gyroscopic lattices, Phys. Rev. B **98**, 174301 (2018).

[80] N. P. Mitchell, L. M. Nash, and W. T. M. Irvine, Realization of a topological phase transition in a gyroscopic lattice, Phys. Rev. B **97**, 100302(R) (2018).

[81] N. P. Mitchell, L. M. Nash, D. Hexner, A. M. Turner, and W. T. M. Irvine, Amorphous topological insulators constructed from random point sets, Nat. Phys. **14**, 380 (2018).

[82] A. Mostafazadeh, Physics of spectral singularities, in *Geometric Methods in Physics*, edited by P. Kielanowski, P. Bieliavsky, A. Odzijewicz, M. Schlichenmaier, and T. Voronov (Springer International Publishing, Cham, 2015), pp. 145–165.

[83] C. M. Bender and S. Boettcher, Real Spectra in Non-Hermitian Hamiltonians Having $\mathcal{PT}$ Symmetry, Phys. Rev. Lett. **80**, 5243 (1998).

[84] M. Fruchart, R. Hanai, P. B. Littlewood, and V. Vitelli, Phase transitions in non-reciprocal active systems, arXiv:2003.13176.

[85] The notion of *PT* symmetry used here generalizes the standard combination of physical spatial inversion and time-reversal symmetry operating on a quantum mechanical Hamiltonian, see [41].

[86] Here, we use TRS in the quantum-mechanical sense.

[87] F. D. M. Haldane, Model for a Quantum Hall Effect without Landau Levels: Condensed-Matter Realization of the "Parity Anomaly", Phys. Rev. Lett. **61**, 2015 (1988).

[88] W. Chen and A. P. Schnyder, Universality classes of topological phase transitions with higher-order band crossing, New J. Phys. **21**, 073003 (2019).

[89] K. Kawabata, T. Bessho, and M. Sato, Classification of Exceptional Points and Non-Hermitian Topological Semimetals, Phys. Rev. Lett. **123**, 066405 (2019).

[90] H. Zhou, J. Y. Lee, S. Liu, and B. Zhen, Exceptional surfaces in PT-symmetric non-hermitian photonic systems, Optica **6**, 190 (2019).

[91] Y. Xiong, Why does bulk boundary correspondence fail in some non-hermitian topological models, J. Phys. Commun. **2**, 035043 (2018).

[92] W. Heiss, The physics of exceptional points, J. Phys. A **45**, 444016 (2012).
[93] T. Yoshida, R. Peters, N. Kawakami, and Y. Hatsugai, Symmetry-protected exceptional rings in two-dimensional correlated systems with chiral symmetry, Phys. Rev. B **99**, 121101(R) (2019).
[94] R. Okugawa and T. Yokoyama, Topological exceptional surfaces in non-hermitian systems with parity-time and parity-particle-hole symmetries, Phys. Rev. B **99**, 041202(R) (2019).
[95] V. Vitelli, N. Xu, M. Wyart, A. J. Liu, and S. R. Nagel, Heat transport in model jammed solids, Phys. Rev. E **81**, 021301 (2010).
[96] We note that the deformed kagome lattice has a mechanical topological polarization [61]. Such a polarization is not necessary for the existence of skin modes.